Photochemical reactions of dissolved organic matter and bromide ions facilitate abiotic formation of manganese oxide solids

Zhenwei Gao, Jing Liu, Charlie Skurie, Yaguang Zhu, and Young-Shin Jun*

Department of Energy, Environmental and Chemical Engineering, Washington University in St. Louis, St. Louis, Missouri 63130, United States

Address: One Brookings Drive, Campus Box 1180

E-mail: ysjun@seas.wustl.edu

Phone: (314) 935-4539

Fax: (314) 696-1223

http://encl.engineering.wustl.edu/

Water Research

Submitted: May 2022

Revised: July 2022

* To whom correspondence should be addressed

Abstract

Manganese (Mn) oxide solids are ubiquitous in nature, acting as both electron donors and acceptors in diverse redox reactions in the environment. Reactions of Mn(III/IV) oxides with dissolved natural organic matter (DOM) are commonly described as reductive dissolutions that generate Mn^{2+}(aq). In this study, we investigated the role of photochemical reactions of DOM in Mn^{2+}(aq) oxidation and the resulting formation of Mn oxide solids. During the photolysis of DOM, reactive intermediates can be generated, including excited triplet state DOM ($^3DOM^*$), hydroxyl radicals ($^\bullet OH$), superoxide radicals ($O_2^{\bullet-}$), hydrogen peroxide, and singlet oxygen. Among these, we found that $O_2^{\bullet-}$ radicals were mainly responsible for Mn oxidation. The solution pH controlled the formation of Mn oxide solids by affecting both Mn^{2+} oxidation by $O_2^{\bullet-}$ during photolysis of DOM and reductive dissolutions of Mn oxide solids by DOM. Further, with the addition of bromide ions (Br^-), reactions between $^3DOM^*$ and Br^-, together with reactions between $^\bullet OH$ and Br^-, can form reactive bromide radicals. The formed Br radicals also promoted Mn oxide formation. In DOM with more aromatic functional groups, more Mn^{2+} was oxidized to Mn oxide solids. This enhanced oxidation could be the result of promoted pathways from charge-transfer state DOM ($DOM^{\bullet+/\bullet-}$) to $O_2^{\bullet-}$. These new observations advance our understanding of natural Mn^{2+} oxidation and Mn(III/IV) oxide formation and highlight the underappreciated oxidative roles of DOM in the oxidation of metal ions in surface water illuminated by sunlight.

Keywords: Abiotic manganese oxidation; Natural organic matter; Reactive oxygen species; Bromide radicals; Photochemistry

1. Introduction

Manganese (Mn) is the second most abundant transition metal in the earth's crust, and is found widely in aquatic and terrestrial environments (Butterfield et al. 2013). Mn has diverse oxidation states (most prevalently Mn(II), Mn(III), and Mn(IV)), and its oxides have high reduction potential (MnO_2/Mn^{2+}, 1.23V) (Stumm and Morgan 1996). In addition, Mn oxide solids are effective scavengers of redox-active species and heavy metals in nature because they can operate as both electron donors and acceptors, and thus play important roles in geochemical element redox cycling, carbon mineralization, and biological metabolisms (Butterfield et al. 2013, Myers and Nealson 1988, Tebo et al. 2004). In nature, most Mn (hydr)oxide solids occur in the Mn(III) and Mn(IV) oxidation states, formed by the oxidation of Mn^{2+}. Regarding the formation of Mn (hydr)oxide solids, previously, the biotic Mn oxidation process was believed to be the dominant oxidative pathway from Mn^{2+}(aq) to Mn(IV) oxide solids in natural systems, because bacteria and fungi accelerate this process by several orders of magnitude compared to abiotic processes (Diaz et al. 2013, Hansel and Francis 2006, Hansel et al. 2012, Learman et al. 2011a, Learman et al. 2011b). On the other hand, abiotic, inorganic oxidation of Mn^{2+}(aq) to Mn(IV) oxide solids has not been considered as a major pathway, owing to its slow and kinetically-controlled process (a half-life of 200–300 days) (Huang et al. 1995). Recently, we discovered fast abiotic oxidation of Mn^{2+} to Mn(IV) by superoxide radicals ($O_2^{\bullet-}$) generated from nitrate photolysis (Jung et al. 2017a), at a rate comparable to biotic processes (Francis and Tebo 2001, Hansel and Francis 2006, Learman et al. 2011a, Learman et al. 2011b), accompanied by the formation of δ-MnO_2 nanosheets (Jung et al. 2017a). This new finding demonstrates that abiotic, inorganic Mn oxidation and solids formation are as important as the biotic process.

The redox active Mn oxide solids can react with dissolved organic matter (DOM), which is a complex matrix of organic matter that are ubiquitous in natural aquatic environments. DOM contains humic substances, such as humic acids (HA) and fulvic acids (FA) with aromatic and carboxylic functional groups (Gaffney et al. 1996). Surface water usually contains 2–10 mgC/L (as dissolved organic carbon) DOM (Lapworth et al. 2008, Nogueira et al. 2017, Sillanpää 2014). Studies thus far have extensively investigated the adsorption of DOM on Mn oxides, and the reduction reactions of solid Mn oxides by DOM. The DOM adsorption on Mn oxides was shown to increase with decreasing pH *via* surface complexation and ligand exchange (Allard et al. 2017, Tipping and Heaton 1983). In addition, enhanced adsorption of DOM on the Mn oxide solids was observed in the presence of Ca^{2+} by decreasing the electrostatic repulsion (Tipping and Heaton 1983). Furthermore, the adsorption of DOM on Mn oxide solids was promoted by higher molecular weight molecules and higher hydrophobicity with more aromatic moieties of DOM that were isolated from the Suwannee River in USA, the Jau River in Brazil, and the Loire River in France (Allard et al. 2017). On the other hand, Mn oxide solids can oxidize DOM while DOM is degraded into small organic matter (Allard et al. 2017, Chorover and Amistadi 2001, Sunda and Kieber 1994). DOM can also affect the reactions between Mn oxides with organic pollutants, such as triclosan and chlorophene in surface water, because DOM can competitively adsorb on and react with MnO_2 (Zhang and Huang 2003). Moreover, sunlight illumination accelerated the reduction of Mn oxide solids by DOM (Bertino and Zepp 1991). So far, most studies have considered DOM to be a reducing agent for Mn oxide solids rather than an oxidative source for Mn^{2+} oxidation processes.

However, DOM can behave as oxidative agents in surface water with sunlight illumination. Sunlight-driven processes can initiate the degradation of DOM, accompanied by the formation of photochemically produced reactive intermediates, such as excited triplet state DOM ($^3DOM^*$), $O_2^{\bullet-}$,

hydrogen peroxide (H_2O_2), hydroxyl radicals ($^{\bullet}OH$), and singlet oxygen ($^1O_2$) (Dalrymple et al. 2010, McNeill and Canonica 2016, Zafiriou 1977, Zafiriou et al. 1984). Then, the generated reactive intermediates can trigger the formation of other reactive radicals. For example, reactive halogen species can be generated by reactions between $^3DOM^*$ and halide ions (Brigante et al. 2014, De Laurentiis et al. 2012, Jammoul et al. 2009, Parker and Mitch 2016) and by reactions between $^{\bullet}OH$ and halide ions (Mopper and Zhou 1990, Neta et al. 1988). This coeffect with halide ions is important because halide ions are abundant in the surface water and some engineered environments. Specifically, the surface water receives large amounts of concentrated flowback efflux that contain concentrated halide ions in desalination processes (Voutchkov 2011, Zhang et al. 2021) and in unconventional oil and gas recovery through hydraulic fracturing (Gregory et al. 2011). Large amounts of soluble organic constituents (for example, 2-butoxyethanol and pyridine) were also produced in the flowback fracturing water (Butkovskyi et al. 2017, Gregory et al. 2011). These effluents are discharged onto the surface and impounded before further treatment and reuse (Gregory et al. 2011, Voutchkov 2011, Zhang et al. 2021). In an ongoing investigation of abiotic Mn oxidation by natural abundant radicals, we have discovered the photo-oxidation of Mn^{2+}(aq) by reactive halogen radicals (mainly from bromide (Br) radicals ($Br^{\bullet}$ and $Br_2^{\bullet-}$)) (Gao et al. 2020, 2021a). The reactive halogen radicals were generated from nitrate photolysis in the presence of naturally abundant halide ions, which facilitated the oxidation of Mn^{2+}(aq) to δ-MnO_2 nanosheets. Similarly, the photolysis of DOM in the presence of halide ions can be an alternative and significant pathway for the generation of reactive oxygen and halogen radicals for inorganic Mn oxidation. However, there is no previous study that examines the impacts of their coexistence on Mn oxidation and resulting formation of Mn oxide solids.

Previously, reactive oxygen species (ROS) and $^3DOM^*$ generated from photolysis of DOM have been highlighted as oxidative agents mainly for organic compounds. For example, ROS and

$^3DOM^*$ can oxidize organic contaminants such as amine drugs (mexiletine, propranolol, and diphenhydramine) and antibiotics (sulfadimethoxine) (Chen et al. 2009, Guerard et al. 2009). However, when it came to the interactions with inorganic ions, such as heavy or transition metal ions, DOM was typically thought to function as chelating agent (Allard et al. 2017, Cabaniss 2011, Pan et al. 2018). Soluble Mn^{3+} species were found to be stabilized by DOM and formed Mn(III)–DOM colloids (Li et al. 2019, Trouwborst et al. 2006). Although a previous study showed the photo-oxidation of Mn^{2+}(aq) to Mn oxides by humic substances and built a kinetic model to fit the experimental results (Nico et al. 2002), information regarding Mn oxidation state, crystalline phase, and morphology of the formed Mn oxides is still unknown. In addition, although sodium chloride was included in the previous work (Nico et al. 2002), the roles of generated chloride (Cl) radicals in Mn oxidation were not considered. Thus, further study is required to fully comprehend the oxidative roles of DOM in photolytic reactions with Mn^{2+}. In particular, we need to examine the coeffect of reactive oxygen and halogen species generated from the reactions between DOM and halide ions on Mn^{2+} oxidation processes. This information will help us better understand the formation of Mn oxide minerals in organic environments.

To examine the underappreciated roles of DOM in Mn oxidation in the natural and engineered water, this study aims to investigate the photolytic oxidation of Mn^{2+}(aq) in the presence of DOM and halide ions. Both reduction reaction of Mn oxide solids by DOM and oxidation reaction of Mn^{2+}(aq) to Mn oxide solids by photolysis of DOM can occur at the same time. Hence, the results here report the net reaction of the reduction and oxidation processes. We found that solution pH significantly impacted the formation of Mn oxide solids by affecting both Mn^{2+} oxidation by $O_2^{\bullet-}$ during photolysis of DOM and reductive dissolutions of Mn oxide solids by DOM. We further investigated the effect of the co-presence of halide ions on Mn^{2+} oxidation. Here, Br^- was chosen as a representative halide ion because we had previously found that although NaBr had a 500-fold

lower concentration than NaCl, at the same IS, more Mn^{2+} was oxidized by Br radicals generated from NaBr than by Cl radicals generated from NaCl, as shown in Fig. S1 (Gao et al. 2020, 2021a). In this study, more Mn oxides were formed in the presence of Br^- compared with that in the absence of Br^- because of reactive Br radicals generated by the reactions between DOM and Br^-. The composition of DOM (e.g., humic acid and fulvic acid) also affected the photo-oxidation rates of Mn^{2+}(aq). This new photo-assisted pathway involving Mn^{2+}(aq) and DOM, can help us better understand how Mn oxide solids are formed in ubiquitous organic-rich surface water systems. In addition, the discoveries in this study will also provide new insights into the impacts of the reactions between DOM and halide ions and their resulting reactive oxygen and halogen species on the oxidation and reduction processes of other transition metal oxides in the environment.

2. Materials and methods

2.1. Chemicals and materials

All chemicals used in this study were at least American Chemical Society grade. Manganese chloride ($MnCl_2$, ≥ 97%, anhydrous) was purchased from Beantown Chemical Co. (NH, USA). Leucoberbelin blue I (LBB, dye content 65%), potassium permanganate ($KMnO_4$, ≥ 99%), superoxide dismutase bovine (SOD, ≥ 90%), and sodium bromide (NaBr, ≥ 99.99%) were purchased from Millipore Sigma, MO. Sodium hydroxide (NaOH, > 97%) and boric acid (H_3BO_3, > 99.5%) were bought from VWR International, LLC to make sodium borate buffer to maintain the solution pH. The Suwannee River natural organic matter (SRNOM, 2R101N), Suwannee River humic acid (SRHA, 2S101H), and Suwannee River fulvic acid (SRFA, 2S101F), purchased from the International Humic Substance Society (IHSS), were used to investigate the effect of DOM composition on Mn^{2+} oxidation. The detailed preparation method of their stock solutions and their composition information, including quantification of carboxyl and aromatic functional groups, are

provided in the Supporting Information (Section 1 and Table S1). Deionized (DI) water (≥ 18.2 MΩ·cm, Barnstead Ultrapure water systems) was used to prepare solutions for all experiments. 0.2 μm polytetrafluoroethylene (PTFE) membrane was bought from VWR International, LLC.

2.2. Photo-oxidation experiments

In a 150 mL quartz reactor, batch photolytic experiments for oxidation of Mn^{2+} were carried out. A 450 W Xenon arc lamp (Newport 6279NS) was used for light illumination, and its light spectrum in the range from 280 to 600 nm is shown in Fig. S2. The light was routed through flowing tap water to filter out near-infrared light and moderate the reactor temperature. 0.1 mM $MnCl_2$ was used as the Mn source. Dissolved Mn concentrations found in natural waters range from 10 to 10,000 μg/L (0.18 μM–0.18 mM) (WHO 1999, 2004, Williams et al. 2013). Although the Mn concentrations employed in this study might be higher than those detected in natural surface waters, the findings can help better comprehend a variety of geochemical scenarios. To understand the effects of pH on Mn^{2+}(aq) oxidation by photolysis of DOM, solutions with and without borate buffer were studied for comparison. For experimental conditions without borate buffer, the solution containing 2 mgC/L (2 mg carbon per liter solution) DOM and 0.1 mM $MnCl_2$ was prepared. Then, to compare the effect of initial pH on Mn oxidation, solution pH was adjusted to 7.0 ± 0.1, 8.0 ± 0.1, or 9.0 ± 0.1 by adding NaOH solution. The experimental pH values are relevant to environmental systems, where the water quality guidelines for pH in freshwater set by the US Environmental Protection Agency (EPA) range from 6.5 to 9.0 (EPA 1986, WHO 2011). For experimental conditions with borate buffer, solution containing 0.1 mM $MnCl_2$, SRNOM, and borate buffer was prepared. Borate buffer solutions, with a pKa of 9.23 (Stoll and Blanchard 2009), were made by adding NaOH into the boric acid solution to reach the desired borate buffer concentrations and pH values (pH 9.0). In this study, 10, 50, and 100 mM borate buffer at pH 9.0

were used to investigate the effects of borate buffer concentration on Mn oxidation. To investigate the effects of concentration of SRNOM on Mn^{2+}(aq) oxidation, 2 and 10 mgC/L of SRNOM were chosen. These concentrations were chosen to mimic environmentally relevant conditions because surface water usually contains 2–10 mgC/L DOM (Lapworth et al. 2008, Nogueira et al. 2017, Sillanpää 2014). To investigate the effects of DOM composition on Mn oxidation, SRNOM, SRHA, and SRFA were used as the DOM sources. For SRNOM concentration analyses, different concentrations of SRNOM solutions were used to obtain a linear calibration curve for SRNOM concentration versus absorbance at 254 nm (Peuravuori and Pihlaja 1997), as shown in Fig. S3. Then, to study the generation of Br radicals for Mn oxidation, we added 1 or 10 mM NaBr in the systems. To determine the corresponding oxidative role of $O_2^{\bullet-}$, SOD was added as the $O_2^{\bullet-}$ scavenger.

To simulate sunlight, we used an Xe Arc lamp, and the prepared solutions were exposed to the light for 6 hours. The samples were taken every hour to track the pH of the solution and the amounts of produced Mn oxide solids. The formed Mn oxide solid products were collected via centrifugation at 10,000 rpm for 30 min. The resulting solid products were then rinsed, resuspended in DI water, and centrifuged at 5,000 rpm for 5 min. The above process was repeated five times to eliminate impurities from the liquid supernatant. The solid products were then dried at room temperature for further characterization.

2.3. Quantification of oxidized Mn oxides

As previously reported (Gao et al. 2021b, Jung et al. 2017a), we quantified the concentrations of formed Mn(III)/Mn(IV) oxide solids by using 0.004 % (w/v) LBB. Specifically, LBB reduced the high oxidation states of Mn(III or IV) in newly formed Mn oxide solids to Mn^{2+}(aq), and then displayed a blue color, whose UV-Vis intensity at 625 nm was proportional to the concentration

of oxidized Mn. For LBB analyses, different concentrations of $KMnO_4$ solutions were used to obtain a linear calibration curve for Mn oxide solids concentration versus UV-Vis absorbance at 625 nm (Fig. S4). Mn(VII) in $KMnO_4$ was reduced to Mn(II) during the redox reaction between $KMnO_4$ and LBB. Thus, a five-electron transfer for each Mn atom was used to obtain the calibration curve between $KMnO_4$ concentration and oxidized LBB intensity at 625 nm. The calculations of Mn oxide concentrations were based on the oxidation states of Mn and electron transfer. Mn(IV) was reduced to Mn(II) when $Mn(IV)O_2$ reacted with LBB, with a two-electron transfer for each Mn atom. Thus, a coefficient of 2.5 was added when calculating the $Mn(IV)O_2$ concentration using the $KMnO_4$ calibration curve owing to the 2.5-time difference in the electron transfer between $Mn(IV)O_2$ and $KMnO_4$. In these measurements, LBB analyses cannot distinguish whether the detected oxidized Mn came from solid phase of Mn oxides or aqueous oxidized Mn. Thus, 0.2 μm PTFE membrane was used to filter out the formed solid phases of Mn oxides and leave aqueous oxidized Mn in the solution. In this way, the existence of aqueous oxidized Mn can be quantified by measuring the solutions after membrane filtration.

2.4. Mn oxides solid phase characterization

To experimentally determine the mineral phases of Mn oxides samples, high-resolution X-ray diffraction (HRXRD, Bruker D8 Advance X-ray diffractometer with Cu Kα radiation (λ = 1.5418 Å)) was utilized. In addition, Mn oxidation states in the Mn oxides samples were characterized by X-ray photoelectron spectroscopy (XPS, PHI 5000 VersaProbe II, UlvacPHI with monochromatic Al Kα radiation (1486.6 eV)). The C 1s peak (284.8 eV) was employed as the reference peak. To determine the ratio of Mn(II), Mn(III) and Mn(IV) in the generated Mn oxide solids, the Mn $2p_{3/2}$ spin orbit was deconvoluted by Mn(II) (640.8eV), Mn(III) (641.8 eV) and Mn(IV) (642.2 eV) by the Gauss-Lorentz fitting method based on previously reported values of the Mn $2p_{3/2}$ spectrum

(Jung et al. 2017b). Sources for the fitting reference values of Mn(II), Mn(III), and Mn(IV) are listed in Table S2. To determine the crystalline phases and to image the morphologies of formed Mn oxide solids, high-resolution transmission electron microscopy (HR-TEM, JEOL-2100F) was used. To prepare HR-TEM samples, after the photochemical reactions, several droplets of formed Mn oxide solution were placed on continuous ultrathin lacey carbon film coated-Cu grids (LC400-Cu-CC-25, Electron Microscopy Science, PA). High-angle annular dark-field scanning transmission electron microscopy (HAADF-STEM) was used to observe the three-dimensional morphology and to conduct element mapping for the formed Mn oxide solids.

3. Results and discussion

3.1. Photochemical oxidation of Mn^{2+}(aq) by SRNOM

During the photolysis of a solution containing 0.1 mM $MnCl_2$ and 2 mgC/L SRNOM at initial pH 9.0 without buffer, 0.82 μM Mn oxide solids (based on Mn(IV) oxidation state) were detected after 1 hr photolysis reaction as measured by the LBB method as shown in the blue curve in Fig. 1A. Because the LBB method cannot distinguish whether the formed oxidized Mn came from solid phase of Mn oxides or aqueous oxidized Mn (e.g., Mn^{3+}(aq)), 0.2 μm PTFE membrane was used to filter out the formed solid phases of Mn oxides and leave aqueous oxidized Mn in the solution. Afterwards, the filtered aqueous solution was measured by LBB again to check the concentration of aqueous oxidized Mn. No oxidized Mn was observed in the purple curve, suggesting that the oxidized Mn only came from the solid phase of Mn oxides. However, the amount of Mn(IV) oxides kept decreasing after 1 hr and became 0 after a 5 hr reaction, and the pH value decreased from initial 9.0 to 7.4 after 1 hr photolysis reaction (Fig. 1B) because DOM served as reducing agents for Mn oxide solids. As shown in Fig. S5, the pH drops mainly resulted from the photo-degradation of DOM and the oxidation of Mn^{2+}(aq), compared with CO_2 dissolution into the solution. Hence,

both the reduction of Mn oxide solids by DOM and the photo-oxidation of Mn^{2+}(aq) by DOM occur simultaneously. According to Allard et al. (2017), when the pH decreased from 7 to 5, the adsorption between DOM on MnO_2 was favored (Allard et al. 2017). Thus, the pH decrease in our study might have enhanced the DOM adsorption on Mn oxide solids and further promoted the kinetics of the reductive dissolution of Mn oxide solids. Moreover, the reductive dissolution of Mn oxide solids is preferred at lower pH values (Xyla et al. 1992). In addition, the decay of $O_2^{\bullet-}$ becomes faster at lower pH values (Ma et al. 2019), which may inhibit Mn oxidation. For these reasons, the reduction kinetics of Mn oxide solids by DOM would be faster than that of the photo-oxidation reaction of Mn^{2+}(aq) after 1 hr (pH < 7.4), resulting in a reductive Mn oxide dissolution-dominant system after 1 hr. During the photolysis reaction of 2 mgC/L SRNOM at initial pH 9, about 36% of SRNOM was degraded after 6 hr reaction (Fig. 1C). In the presence of 0.1mM $MnCl_2$, 49% of SRNOM was degraded after 6 hr reaction, suggesting that the presence of $MnCl_2$ facilitated the photo-degradation of SRNOM. Although we did not examine effects of light intensity on the photolysis of DOM and subsequent Mn^{2+} oxidation in this study, different light intensities can affect these processes, systematic future studies are, therefore, warranted.

To better understand the effects of pH on Mn oxidation induced by the photolysis of DOM, the same recipe solution (i.e., 0.1 mM $MnCl_2$ and 2 mgC/L SRNOM) was made but adjusted at initial pH 8.0 or 7.0 rather than pH 9.0. As shown in Fig. 1A, a very small amount of Mn oxides was detected at 15 min (pH ~7.5 ± 0.1). After 15 min, the reduction process of Mn oxides by SRNOM was prevailing because the pH of the solution further decreased. The formed Mn oxides reductively dissolved to Mn^{2+}(aq). No oxidized Mn was observed in the orange curve, suggesting that the oxidized Mn only came from the solid phase of Mn oxides, which was the same as initial pH 9 condition. No Mn oxides were detected after 1 hr. Under the condition of initial pH 7.0, no

Mn oxidation was observed. Thus, the oxidation of Mn^{2+}(aq) by SRDOM was dominant only when pH was higher than 7.5 ± 0.1.

3.2. Mn^{2+}oxidation at a controlled pH with buffer

We have demonstrated that the net production of Mn oxide solids from the reductive dissolution of Mn oxide solids by DOM and the photo-oxidation of Mn^{2+}(aq) by DOM were affected by the solution pH. Because the pH values of the surface water generally maintain an overall steady pH, borate buffer with pH of 9.0 was used in the rest of this study to mimic environmental-relevant conditions. As shown in Fig. 2A,B, the quantity of generated Mn oxides continuously increased during the photolysis of solution containing 0.1 mM $MnCl_2$, 2 mgC/L SRNOM, and 10 mM borate buffer and the pH is maintained at pH ~9.0. After 6 h reaction, about 12.3 ± 0.7 μM of Mn oxides formed (based on Mn(IV) oxidation state).

During the photo-oxidation of natural dissolved organic matter, $^3DOM^*$, $DOM^{\bullet+/\bullet-}$, $^\bullet OH$, $O_2^{\bullet-}$, H_2O_2, and $^1O_2$ can be generated (Dalrymple et al. 2010, McNeill and Canonica 2016, Zafiriou 1977, Zafiriou et al. 1984). As shown in Scheme 1A, both oxidation of Mn^{2+}(aq) by $O_2^{\bullet-}$ during the photolysis of DOM and reduction of Mn oxide solids by DOM occurred. Please note that although DOM can act as a scavenger for free radicals, such as $^\bullet OH$ and $^1O_2$ (Cory et al. 2009, Vione et al. 2006), in this study, as a good starting point to understand the system, we focus on the net effects of ROS on Mn oxidation. Scheme 1B,C summarize the detailed generation pathways of the reactive species by either energy transfer or charge (electron) transfer reactions. First, DOM is excited by photon absorption and transitions to excited singlet state of DOM ($^1DOM^*$), then $^3DOM^*$ is generated by intersystem crossing from the $^1DOM^*$ (Step 2). The formed $^3DOM^*$ can react with O_2 to form $^1O_2$ via energy transfer (Step 3). $^3DOM^*$ can also be oxidized by O_2 and generate $O_2^{\bullet-}$ (Step 4). For charge transfer processes, $DOM^{\bullet+/\bullet-}$ behaves as an intramolecular

charge-transfer complex with a diradical character. It is produced by direct charge transfer absorbance from DOM (Step 5), as well as intramolecular electron transfer from $^{1}DOM^{*}$ and $^{3}DOM^{*}$ (Steps 6 and 7). $DOM^{\bullet+/\bullet-}$ can react with O_2 to produce $O_2^{\bullet-}$ via electron transfer (Step 8). Moreover, $^{\bullet}OH$ can be formed through oxidation of H_2O by $^{3}DOM^{*}$ (Step 9), as well as through the chain reactions from $O_2^{\bullet-}$ to H_2O_2, and from H_2O_2 to $^{\bullet}OH$ (Step 10). These reactive intermediates can potentially effect Mn^{2+} oxidation. We have systematically proved that $^{\bullet}OH$ radicals contribute little to Mn oxide formation (Gao et al. 2021b). In the presence of the $^{\bullet}OH$ scavenger *tert*-butyl alcohol, Mn^{2+} oxidation during nitrate photolysis was promoted rather than inhibited, demonstrating that $^{\bullet}OH$ radicals played a little role in oxidizing Mn^{2+} (Gao et al. 2021b). In the presence of SOD, a $O_2^{\bullet-}$ scavenger, Mn^{2+} oxidation during nitrate photolysis was not observed, proving that $O_2^{\bullet-}$ radicals were mainly responsible for Mn^{2+} oxidation (Gao et al. 2021b, Jung et al. 2017a). The reason might be that $^{\bullet}OH$ radicals have a much shorter diffusion length and half-life (nanoseconds) compared with $O_2^{\bullet-}$ (seconds) (Krumova and Cosa 2016, Levy et al. 2019). As for other ROS, H_2O_2 was considered as a reductant rather than an oxidant for Mn oxide solids (Godwin et al. 2020). Nico et al. (2002) reported the oxidation of Mn^{2+}(aq) to Mn(III) by $O_2^{\bullet-}$ and $^{1}O_2$ from photolysis of humic substances. However, only 4% of the formed Mn(III) came from $^{1}O_2$, while the rest came from $O_2^{\bullet-}$ (Nico et al. 2002). Thus, in this study, we hypothesized that $O_2^{\bullet-}$ were the main oxidants responsible for Mn^{2+} oxidation. To confirm the hypothesis, SOD was used as the specific scavenger of $O_2^{\bullet-}$ to determine the corresponding role of $O_2^{\bullet-}$, using our previous methodology (Gao et al. 2021b, Jung et al. 2017a). During the photolysis of the solution containing 0.1 mM $MnCl_2$, 2 mgC/L SRNOM, and 10 mM borate buffer, by adding 0.5 μM SOD, Mn oxidation was not observed, as shown in Fig. 2A. In Fig. S6, no Mn oxidation was observed during the photolysis of a solution containing 0.1 mM $MnCl_2$ and 10 mM borate buffer, indicating that borate buffer did not oxidize Mn^{2+}(aq) and the oxidized Mn resulted from the photolysis of

SRNOM. The results proved that $O_2^{\bullet-}$ radicals were mainly responsible for Mn oxidation among all ROS, which is similar with biotic Mn oxidation by extracellular $O_2^{\bullet-}$ radicals (Diaz et al. 2013, Hansel et al. 2012, Learman et al. 2011a, Learman et al. 2011b).

During the photo-oxidation of Mn^{2+}(aq) to Mn(IV) oxide solids, Mn^{3+}(aq) can form as an intermediate product (Jung et al. 2017a). The Mn^{3+}(aq) is favored to interact with strong ligands to form stable complexation (Oldham et al. 2017), and borate buffer might complex with Mn^{3+}(aq). In our previous study, we found pyrophosphate buffer can complex with Mn^{3+}(aq) and affect Mn oxidation processes (Jung et al. 2017b). To test the existence of oxidized Mn^{3+}(aq) in the solution, 0.2 μm PTFE membrane was used to filter out the formed Mn oxide solids. As shown in Fig. S7, no oxidized Mn in the solution was detected after solid phases of oxidized Mn were removed, validating the hypothesis that the oxidized Mn in LBB measurements are Mn oxide solids. Thus, complexation between borate buffer and Mn^{3+}(aq) would not be significant or exist. In addition, Nico et al. (2002) stated that borate did not complex with Mn^{2+}(aq) (Nico et al. 2002). However, it is still possible that borate may affect Mn oxidation kinetics by complexing with DOM or degraded products of DOM. To investigate the effects of borate buffer concentration on Mn oxidation, we have tested the Mn oxidation with 50 or 100 mM borate buffers at pH 9.0. As shown in Fig. S8, less Mn oxidation was observed with higher concentrations of borate buffer while the pH remained overall steady between 8.5–9.0 during the 6 hr photolytic reactions for all conditions. Previously, borate was found to form covalent complexes with mono- and oligosaccharides, nucleic acid ribose moieties, pyridine nucleotides, and other gem-diols (Stoll and Blanchard 2009). Thus, although borate buffer had low affinity to complex with aqueous Mn, it may favorably form complexes with DOM or degraded product of DOM during the photolysis, affecting the kinetics of generation of reactive oxidative intermediate species and further affecting Mn oxidation. To

minimize the effect of borate buffer concentration on Mn oxidation, the concentration of borate buffer was fixed (10 mM) in this study.

3.3. Determination of Mn oxide solids formed by DOM photolysis

High-resolution X-ray diffraction measurements were used to characterize the crystalline phases of Mn oxides formed by photolysis of a solution containing 0.1 mM $MnCl_2$, 2 mgC/L SRNOM, and 10 mM borate buffer at pH about 9.0 for 6 hr reaction. As shown in Fig. 2C, 2θ peak value of 18.9° indicated that λ-MnO_2 (ICDD PDF-4 #00-044-0992) had formed. A tiny XRD peak at a 2θ of 28.3° suggested that pyrolusite β-MnO_2 (ICDD PDF-4 #00-004-0591) had formed. Moreover, a broad XRD peak at a 2θ of 12.4° suggested the crystalline phase δ-MnO_2 (ICDD PDF-4 #00-043-1456). On the other hand, α-MnO_2 (ICDD PDF-4 #00-042-1348) has characteristic peaks at 2θ values of both 12.8° and 28.9°, which closely correspond to the peaks of the measured sample. Thus, the measured sample can contain α-MnO_2 as well. DOM is a complex matrix containing various components, which possibly led to the formation of diverse crystalline phases of Mn oxides during photolysis of DOM.

The X-ray photoelectron spectroscopy (XPS) image in Fig. 2D suggested that formed solid Mn oxides contain 82.8% Mn(IV) and 15.5% Mn(III) with a very small fraction (1.7%) of Mn(II), resulting in an average oxidation state of 3.81, which is slightly higher than that of δ-MnO_2 generated from nitrate photolysis (3.73) (Gao et al. 2021b). Because Mn average oxidation state was lower than 4 in the XPS results, the actual concentrations of Mn oxide solids could be slightly higher than the values measured by LBB method in Fig. 2A. As shown in Fig. 3A,B, a three-dimensional structure of the Mn oxides was obtained in HAADF-STEM images. Both flake and rod morphologies of Mn oxides were observed. The STEM-EDX spectra and elemental mapping of Mn and O in Fig. 3C-E collected from Fig. 3B confirmed the formation of Mn oxides. In the

selected area electron diffraction (SAED) patterns in Fig. 3F, the ring pattern with a d-spacing of 0.47 nm indicated the (111) plane of λ-MnO_2. In addition, the ring pattern with a d-spacing of 0.31 nm suggested the (110) of β-MnO_2 or (310) of α-MnO_2. The (001) plane of δ-MnO_2 was not observed because it was too close to the bright beam center. Compared with the δ-MnO_2 nanosheets formed by nitrate photolysis (Fig. S9) that we previously observed (Gao et al. 2021b, Jung et al. 2017a), different crystalline structures, oxidation states, and morphologies of Mn oxides were formed by the photolysis of DOM, which may result from the variance of the chemical environments for Mn oxidation.

3.4. Effects of DOM concentration and bromide ions on Mn^{2+} oxidation

Theoretically, the higher concentration of DOM, the more $O_2^{\bullet-}$ will be generated, which promotes the oxidation of Mn^{2+}(aq). However, the reduction of Mn oxide solids by DOM will also be enhanced with a higher DOM concentration. It is unclear which process is dominant with different DOM concentrations. The DOM concentration in the surface water usually ranges from 2 to 10 mgC/L (Lapworth et al. 2008, Nogueira et al. 2017, Sillanpää 2014). In this study, both 2 and 10 mgC/L of DOM were utilized to study the effects of DOM concentration on Mn oxidation at pH 9. As shown in Fig. 4, 2 mM SRNOM (orange curve) system formed 12.3 μM of Mn oxide solids (based on Mn(IV) oxidation state) after 6 hr reaction, while 10 mgC/L SRNOM (red curve) formed 26.0 μM of Mn oxide solids, indicating the oxidation of Mn^{2+}(aq) is prevailing with a higher DOM concentration at pH 9.

In addition, the effects of DOM on Mn^{2+} oxidation were investigated in the presence of Br^-. Halide ions are ubiquitous in natural and engineered environments. In our previous study (Gao et al. 2020, 2021a), we investigated the different contributions of Cl and Br radicals to Mn^{2+} oxidation. In that study, 500 mM NaCl and 1mM NaBr were investigated as a representative for Cl^- and Br^-,

respectively (Gao et al. 2020, 2021a). Despite the fact that NaBr had a 500-fold lower concentration than NaCl, at the same ionic strength, Br radicals generated by NaBr oxidized more Mn^{2+} than Cl radicals generated by NaCl, as shown in Fig. S1 (Gao et al. 2020, 2021a). Thus, only bromide ions were investigated, and Cl ions were not included in this study. For this test, we used 1 and 10 mM NaBr to study the effect of DOM and bromide ions on the photochemical Mn oxidation process. These concentrations were chosen to mimic environmentally relevant conditions. The concentration of Br^- greatly increases in the surface water that receives large amounts of concentrated flowback efflux in unconventional oil and gas recovery (Gregory et al. 2011). Br concentrations can reach about 1.8 g/L (22.5 mM) in Marcellus and Fayetteville hydraulic fracturing flowback fluids, 1 g/L (12.5 mM) in effluents from Pennsylvania brine treatment sites, and 40 mg/L (0.5 mM) in contaminated surface waters from effluent disposal sites (Harkness et al. 2015). As shown in Fig. 3D, $^{\bullet}OH$ can oxidize Br^- to form reactive Br radicals (Step 12). In addition, $^3DOM^*$ can directly oxidize Br^- to form reactive Br radicals (Step 11). Fig. 4A shows Mn oxidation in the presence of additional 1 mM NaBr (blue curve). The Mn oxidation amount was slightly higher than that in the condition without bromide (orange curve) because of the formation of reactive Br radicals. When increasing the concentration of NaBr from 1 to 10 mM (green curve), Mn oxidation was further enhanced. However, compared with increasing NaBr concentration, Mn oxidation kinetics was greatly promoted with the increment of SRNOM concentration. When the concentration of SRNOM increased from 2 to 10 mgC/L and in the presence of 10 mM NaBr (black curve), the Mn oxidation amount almost doubled, increasing from 18.0 to 32.7 μM after 6 hr reaction, which resulted from more generation of both $O_2^{\bullet-}$ and reactive Br radicals under the condition of higher SRNOM concentration. The pH values for all conditions remained between 8.5–9.0 during the reaction (Fig. 4B).

3.5. Effects of DOM composition on Mn^{2+} oxidation

Because DOM is a mixture of humic substances containing carboxyl and aromatic functional groups, it is important to understand the effects of the DOM composition on Mn^{2+}oxidation. The composition of DOM was found to affect its photochemically produced reactive intermediates (Berg et al. 2019, Bodhipaksha et al. 2015, Maizel and Remucal 2017). The generation of $^3DOM^*$ and $^1O_2$ was found to be most significantly connected with more saturated chemical forms of microbially generated DOM (Maizel et al. 2017, McCabe and Arnold 2017).

To investigate the effects of DOM composition on Mn oxidation, SRNOM, SRHA, and SRFA were used. As shown in Table S1, the quantity of the carboxyl functional group decreases in the following order: SRNOM ≈ SRFA > SRHA. On the other hand, the aromatic functional group decreases as follows: SRHA > SRFA > SRNOM (Driver and Perdue 2014, Ritchie and Perdue 2003). During the photolysis of solutions containing 0.1 mM $MnCl_2$, 10 mM borate buffer, and 10 mgC/L SRHA, SRFA, or SRNOM, the quantity of generated Mn oxides decreased as SRHA > SRFA > SRNOM, as shown in Fig. 4A. Berg et al. (2019) reported that a larger amount of $^{\bullet}OH$ was generated from aromatic and oxygenated DOM, while a smaller amount of $^3DOM^*$ and $^1O_2$ were measured, indicating that DOM with greater amounts of aromatic functional groups promotes the charge transfer process (Berg et al. 2019), as shown in Fig. 4C. In addition, compared with $^3DOM^*$ (energy transfer), $DOM^{\bullet+}/^{\bullet-}$ (charge transfer) is dominant in $O_2^{\bullet-}$ production (Le Roux et al. 2021, Ma et al. 2020, Zhang and Blough 2016). Thus, humic acid, with a higher amount of aromatic functional groups than fulvic acid, generated more $O_2^{\bullet-}$, resulting in more Mn oxidation, as represented in Fig. 4A. Because pH did not change much during the Mn oxidation (Fig. 4B), we excluded the possibility of pH variance as an explanation for the difference in the extent of Mn oxidation.

4. Conclusions

In this study, we explored the abiotic Mn oxidation pathways by examining the roles of DOM and bromide ions in Mn photo-oxidation. DOM can act as an oxidative agent for Mn^{2+}(aq) oxidation processes during photolysis by producing $O_2^{\bullet-}$. We found the solution pH influenced the formation of Mn oxide solids during the photolysis of DOM. The oxidation processes were dominant at relatively high pH (pH > 7.5 ± 0.1). However, when pH became lower (pH < 7.5 ± 0.1), reductive dissolution of Mn oxide solids to Mn^{2+}(aq) was more favored. When pH was maintained at 9.0 by pH buffer, the generation of Mn oxide solids kept increasing. Because the complex and various components of DOM affected the Mn oxidation processes, various crystalline structures of Mn oxide solids were observed, which provides an improved understanding of diversity of natural Mn oxide solids.

Furthermore, this study enables a deeper understanding of the impacts of Br^- and reactive Br radicals on photochemical Mn oxidation processes in the presence of organic matter. In the addition of Br^-, Br radicals can be formed, which further promoted Mn oxidation. The coeffect of Br^- and natural organic compounds on Mn oxidation in this study emphasizes the unforeseen impact of reactive oxygen and halogen radicals and predicts their reactions with heavy metal ions (e.g., Fe^{2+}, As^{3+}, and Cr^{3+}) other than Mn in organic-rich environments.

Declaration of competing interest

The authors declare that they have no known competing financial interests or personal relationships that could have appeared to influence the work reported in this paper.

Acknowledgements

The authors are grateful for the support received from the National Science Foundation's Environmental Chemical Sciences program (CHE-1905077). The authors would like to acknowledge the Nano Research Facility (NRF) of Washington University in St. Louis for use of the TOC Analyzer and Institute of Materials Science & Engineering (IMSE) for the use of XPS and HR-TEM. The authors thank the members of the Environmental NanoChemistry Group for valuable discussions.

Supplementary materials

All the relevant data supporting the findings of the study are available in the manuscript and Supplementary Information.

References

Allard, S., Gutierrez, L., Fontaine, C., Croué, J.-P. and Gallard, H. (2017) Organic matter interactions with natural manganese oxide and synthetic birnessite. Science of the Total Environment 583, 487-495.

Berg, S.M., Whiting, Q.T., Herrli, J.A., Winkels, R., Wammer, K.H. and Remucal, C.K. (2019) The role of dissolved organic matter composition in determining photochemical reactivity at the molecular level. Environmental Science & Technology 53(20), 11725-11734.

Bertino, D.J. and Zepp, R.G. (1991) Effects of solar radiation on manganese oxide reactions with selected organic compounds. Environmental Science & Technology 25(7), 1267-1273.

Bodhipaksha, L.C., Sharpless, C.M., Chin, Y.-P., Sander, M., Langston, W.K. and MacKay, A.A. (2015) Triplet photochemistry of effluent and natural organic matter in whole water and isolates from effluent-receiving rivers. Environmental Science & Technology 49(6), 3453-3463.

Brigante, M., Minella, M., Mailhot, G., Maurino, V., Minero, C. and Vione, D. (2014) Formation and reactivity of the dichloride radical ($Cl_2^{-\bullet}$) in surface waters: A modelling approach. Chemosphere 95, 464-469.

Butkovskyi, A., Bruning, H., Kools, S.A., Rijnaarts, H.H. and Van Wezel, A.P. (2017) Organic pollutants in shale gas flowback and produced waters: identification, potential ecological impact, and implications for treatment strategies. Environmental Science & Technology 51(9), 4740-4754.

Butterfield, C.N., Soldatova, A.V., Lee, S.-W., Spiro, T.G. and Tebo, B.M. (2013) Mn(II, III) oxidation and MnO_2 mineralization by an expressed bacterial multicopper oxidase. Proceedings of the National Academy of Sciences 110(29), 11731-11735.

Cabaniss, S.E. (2011) Forward modeling of metal complexation by NOM: II. Prediction of binding site properties. Environmental Science & Technology 45(8), 3202-3209.

Chen, Y., Hu, C., Hu, X. and Qu, J. (2009) Indirect photodegradation of amine drugs in aqueous solution under simulated sunlight. Environmental Science & Technology 43(8), 2760-2765.

Chorover, J. and Amistadi, M.K. (2001) Reaction of forest floor organic matter at goethite, birnessite and smectite surfaces. Geochimica et Cosmochimica Acta 65(1), 95-109.

Cory, R.M., Cotner, J.B. and McNeill, K. (2009) Quantifying interactions between singlet oxygen and aquatic fulvic acids. Environmental Science & Technology 43(3), 718-723.

Dalrymple, R.M., Carfagno, A.K. and Sharpless, C.M. (2010) Correlations between dissolved organic matter optical properties and quantum yields of singlet oxygen and hydrogen peroxide. Environmental Science & Technology 44(15), 5824-5829.

De Laurentiis, E., Minella, M., Maurino, V., Minero, C., Mailhot, G., Sarakha, M., Brigante, M. and Vione, D. (2012) Assessing the occurrence of the dibromide radical ($Br_2^{-\bullet}$) in natural waters: Measures of triplet-sensitised formation, reactivity, and modelling. Science of the Total Environment 439, 299-306.

Diaz, J.M., Hansel, C.M., Voelker, B.M., Mendes, C.M., Andeer, P.F. and Zhang, T. (2013) Widespread production of extracellular superoxide by heterotrophic bacteria. science, 1237331.

Driver, S.J. and Perdue, E.M. (2014) Advances in the Physicochemical Characterization of Dissolved Organic Matter: Impact on Natural and Engineered Systems, pp. 75-86, ACS Publications.

EPA (1986) Quality criteria for water.

Francis, C.A. and Tebo, B.M. (2001) Enzymatic manganese(II) oxidation by a marine α-proteobacterium. Applied and Environmental Microbiology 67(9), 4024-4029.

Gaffney, J.S., Marley, N.A. and Clark, S.B. (1996) Humic and fulvic acids and organic colloidal materials in the environment.

Gao, Z., Skurie, C. and Jun, Y.-S. (2020) Effects of halide ions on photochemically-induced abiotic formation of Mn oxides. American Chemical Society National Meeting.

Gao, Z., Skurie, C. and Jun, Y.-S. (2021a) Effects of reactive halogen species on the formation of photochemically-induced abiotic MnIV oxides. American Chemical Society National Meeting.

Gao, Z., Zhang, D. and Jun, Y.-S. (2021b) Does *tert*-butyl alcohol really terminate the oxidative activity of $^{\bullet}OH$ in inorganic redox chemistry? Environmental Science & Technology 55(15), 10442-10450.

Godwin, C.M., Zehnpfennig, J.R. and Learman, D.R. (2020) Biotic and abiotic mechanisms of manganese(II) oxidation in Lake Erie. Frontiers in Environmental Science 8, 57.

Gregory, K.B., Vidic, R.D. and Dzombak, D.A. (2011) Water management challenges associated with the production of shale gas by hydraulic fracturing. Elements 7(3), 181-186.

Guerard, J.J., Chin, Y.-P., Mash, H. and Hadad, C.M. (2009) Photochemical fate of sulfadimethoxine in aquaculture waters. Environmental Science & Technology 43(22), 8587-8592.

Hansel, C.M. and Francis, C.A. (2006) Coupled photochemical and enzymatic Mn(II) oxidation pathways of a planktonic Roseobacter-like bacterium. Applied and Environmental Microbiology 72(5), 3543-3549.

Hansel, C.M., Zeiner, C.A., Santelli, C.M. and Webb, S.M. (2012) Mn(II) oxidation by an ascomycete fungus is linked to superoxide production during asexual reproduction. Proceedings of the National Academy of Sciences 109(31), 12621-12625.

Harkness, J.S., Dwyer, G.S., Warner, N.R., Parker, K.M., Mitch, W.A. and Vengosh, A. (2015) Iodide, bromide, and ammonium in hydraulic fracturing and oil and gas wastewaters: environmental implications. Environmental Science & Technology 49(3), 1955-1963.

Huang, C.P., O'Melia, C.R. and Morgan, J.J. (1995) Aquatic Chemistry: interfacial and interspecies processes, American Chemical Society.

Jammoul, A., Dumas, S., D'anna, B. and George, C. (2009) Photoinduced oxidation of sea salt halides by aromatic ketones: a source of halogenated radicals. Atmospheric Chemistry and Physics 9(13), 4229-4237.

Jung, H., Chadha, T.S., Kim, D., Biswas, P. and Jun, Y.-S. (2017a) Photochemically assisted fast abiotic oxidation of manganese and formation of δ-MnO_2 nanosheets in nitrate solution. Chemical Communications 53(32), 4445-4448.

77 Jung, H., Chadha, T.S., Min, Y., Biswas, P. and Jun, Y.-S. (2017b) Photochemically-assisted
78 synthesis of birnessite nanosheets and their structural alteration in the presence of pyrophosphate.
79 ACS Sustainable Chemistry & Engineering 5(11), 10624-10632.

80 Krumova, K. and Cosa, G. (2016) Overview of reactive oxygen species.

81 Lapworth, D.J., Gooddy, D., Butcher, A. and Morris, B. (2008) Tracing groundwater flow and
82 sources of organic carbon in sandstone aquifers using fluorescence properties of dissolved organic
83 matter (DOM). Applied Geochemistry 23(12), 3384-3390.

84 Le Roux, D.M., Powers, L.C. and Blough, N.V. (2021) Photoproduction rates of one-electron
85 reductants by chromophoric dissolved organic matter via fluorescence spectroscopy: comparison
86 with superoxide and hydrogen peroxide rates. Environmental Science & Technology 55(17),
87 12095-12105.

88 Learman, D., Voelker, B., Vazquez-Rodriguez, A. and Hansel, C. (2011a) Formation of
89 manganese oxides by bacterially generated superoxide. Nature Geoscience 4(2), 95-98.

90 Learman, D., Wankel, S., Webb, S., Martinez, N., Madden, A. and Hansel, C. (2011b) Coupled
91 biotic–abiotic Mn(II) oxidation pathway mediates the formation and structural evolution of
92 biogenic Mn oxides. Geochimica et Cosmochimica Acta 75(20), 6048-6063.

93 Levy, M., Chowdhury, P.P. and Nagpal, P. (2019) Quantum dot therapeutics: a new class of radical
94 therapies. Journal of Biological Engineering 13(1), 48.

95 Li, Q., Xie, L., Jiang, Y., Fortner, J.D., Yu, K., Liao, P. and Liu, C. (2019) Formation and stability
96 of NOM-Mn(III) colloids in aquatic environments. Water Research 149, 190-201.

97 Ma, J., Nie, J., Zhou, H., Wang, H., Lian, L., Yan, S. and Song, W. (2020) Kinetic consideration
98 of photochemical formation and decay of superoxide radical in dissolved organic matter solutions.
99 Environmental Science & Technology 54(6), 3199-3208.

100 Ma, J., Zhou, H., Yan, S. and Song, W. (2019) Kinetics studies and mechanistic considerations on
101 the reactions of superoxide radical ions with dissolved organic matter. Water Research 149, 56-64.

102 Maizel, A.C., Li, J. and Remucal, C.K. (2017) Relationships between dissolved organic matter
103 composition and photochemistry in lakes of diverse trophic status. Environmental Science &
104 Technology 51(17), 9624-9632.

105 Maizel, A.C. and Remucal, C.K. (2017) Molecular composition and photochemical reactivity of
106 size-fractionated dissolved organic matter. Environmental Science & Technology 51(4), 2113-
107 2123.

108 McCabe, A.J. and Arnold, W.A. (2017) Reactivity of triplet excited states of dissolved natural
109 organic matter in stormflow from mixed-use watersheds. Environmental Science & Technology
110 51(17), 9718-9728.

111 McNeill, K. and Canonica, S. (2016) Triplet state dissolved organic matter in aquatic
112 photochemistry: reaction mechanisms, substrate scope, and photophysical properties.
113 Environmental Science: Processes & Impacts 18(11), 1381-1399.

114 Mopper, K. and Zhou, X. (1990) Hydroxyl radical photoproduction in the sea and its potential
115 impact on marine processes. Science 250(4981), 661-664.

Myers, C.R. and Nealson, K.H. (1988) Bacterial manganese reduction and growth with manganese oxide as the sole electron acceptor. science 240(4857), 1319-1321.

Neta, P., Huie, R.E. and Ross, A.B. (1988) Rate constants for reactions of inorganic radicals in aqueous solution. Journal of Physical and Chemical Reference Data 17(3), 1027-1284.

Nico, P.S., Anastasio, C. and Zasoski, R.J. (2002) Rapid photo-oxidation of Mn(II) mediated by humic substances. Geochimica et Cosmochimica Acta 66(23), 4047-4056.

Nogueira, L.S., Bianchini, A., Smith, S., Jorge, M.B., Diamond, R.L. and Wood, C.M. (2017) Physiological effects of five different marine natural organic matters (NOMs) and three different metals (Cu, Pb, Zn) on early life stages of the blue mussel (Mytilus galloprovincialis). PeerJ 5, e3141.

Oldham, V.E., Mucci, A., Tebo, B.M. and Luther III, G.W. (2017) Soluble Mn(III)–L complexes are abundant in oxygenated waters and stabilized by humic ligands. Geochimica et Cosmochimica Acta 199, 238-246.

Pan, Y., Garg, S., Waite, T.D. and Yang, X. (2018) Copper inhibition of triplet-induced reactions involving natural organic matter. Environmental Science & Technology 52(5), 2742-2750.

Parker, K.M. and Mitch, W.A. (2016) Halogen radicals contribute to photooxidation in coastal and estuarine waters. Proceedings of the National Academy of Sciences 113(21), 5868-5873.

Peuravuori, J. and Pihlaja, K. (1997) Molecular size distribution and spectroscopic properties of aquatic humic substances. Analytica Chimica Acta 337(2), 133-149.

Ritchie, J.D. and Perdue, E.M. (2003) Proton-binding study of standard and reference fulvic acids, humic acids, and natural organic matter. Geochimica et Cosmochimica Acta 67(1), 85-96.

Sillanpää, M. (2014) Natural organic matter in water: Characterization and treatment methods, Butterworth-Heinemann.

Stoll, V.S. and Blanchard, J.S. (2009) Buffers: principles and practice. Methods in Enzymology 463, 43-56.

Stumm, W. and Morgan, J. (1996) Oxidation and reduction; equilibria and microbial mediation. Aquatic Chemistry. 3rd edn. Wiley-Interscience, USA 425, 511.

Sunda, W.G. and Kieber, D.J. (1994) Oxidation of humic substances by manganese oxides yields low-molecular-weight organic substrates. Nature 367(6458), 62-64.

Tebo, B.M., Bargar, J.R., Clement, B.G., Dick, G.J., Murray, K.J., Parker, D., Verity, R. and Webb, S.M. (2004) Biogenic manganese oxides: properties and mechanisms of formation. Annu. Rev. Earth Planet. Sci. 32, 287-328.

Tipping, E. and Heaton, M. (1983) The adsorption of aquatic humic substances by two oxides of manganese. Geochimica et Cosmochimica Acta 47(8), 1393-1397.

Trouwborst, R.E., Clement, B.G., Tebo, B.M., Glazer, B.T. and Luther, G.W. (2006) Soluble Mn(III) in suboxic zones. Science 313(5795), 1955-1957.

Vione, D., Falletti, G., Maurino, V., Minero, C., Pelizzetti, E., Malandrino, M., Ajassa, R., Olariu, R.-I. and Arsene, C. (2006) Sources and sinks of hydroxyl radicals upon irradiation of natural water samples. Environmental Science & Technology 40(12), 3775-3781.

Voutchkov, N. (2011) Overview of seawater concentrate disposal alternatives. Desalination 273(1), 205-219.

WHO (1999) Concise international chemical assessment document 12, Manganese and its compounds, World Health Organization.

WHO (2004) Concise international chemical assessment document 63, Manganese and its Compounds: Environmental Aspects, World Health Organization.

WHO (2011) Nitrate and nitrite in drinking-water, World Health Organization

Williams, M., Todd, G.D., Roney, N., Crawford, J., Coles, C., McClure, P.R., Garey, J.D., Zaccaria, K. and Citra, M. (2013) Toxicological profile for manganese.

Xyla, A.G., Sulzberger, B., Luther III, G.W., Hering, J.G., Van Cappellen, P. and Stumm, W. (1992) Reductive dissolution of manganese(III, IV) (hydr)oxides by oxalate: The effect of pH and light. Langmuir 8(1), 95-103.

Zafiriou, O.C. (1977) Marine organic photochemistry previewed. Marine Chemistry 5(4-6), 497-522.

Zafiriou, O.C., Joussot-Dubien, J., Zepp, R.G. and Zika, R.G. (1984) Photochemistry of natural waters. Environmental Science & Technology 18(12), 358A-371A.

Zhang, C., Shi, Y., Shi, L., Li, H., Li, R., Hong, S., Zhuo, S., Zhang, T. and Wang, P. (2021) Designing a next generation solar crystallizer for real seawater brine treatment with zero liquid discharge. Nature communications 12(1), 1-10.

Zhang, H. and Huang, C.-H. (2003) Oxidative transformation of triclosan and chlorophene by manganese oxides. Environmental Science & Technology 37(11), 2421-2430.

Zhang, Y. and Blough, N.V. (2016) Photoproduction of one-electron reducing intermediates by chromophoric dissolved organic matter (CDOM): relation to O_2^- and H_2O_2 photoproduction and CDOM photooxidation. Environmental Science & Technology 50(20), 11008-11015.

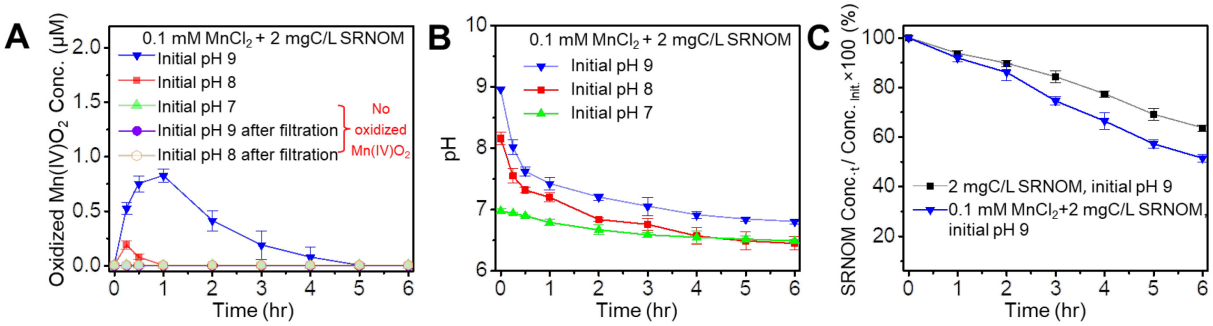

180

181 **Fig. 1.** Photochemical Mn oxidation by SRNOM. (A) Oxidized Mn concentration and (B) pH
182 values during photolysis of solution containing 0.1 mM $MnCl_2$, 2 mgC/L SRNOM at initial pH
183 9.0, 8.0, or 7.0. For initial pH 9.0 and 8.0 conditions, 0.2 μm PTFE membrane was used to filter
184 out all the solids in the solution. The aqueous oxidized Mn in the filtered solution was not detected.
185 (C) Percentages of the concentration decrease of SRNOM with the elapse of time for photolysis
186 of solution containing 2 mgC/L SRNOM with or without 0.1 mM $MnCl_2$ at initial pH 9. Error bars
187 represent the standard deviation from at least duplicate tests.

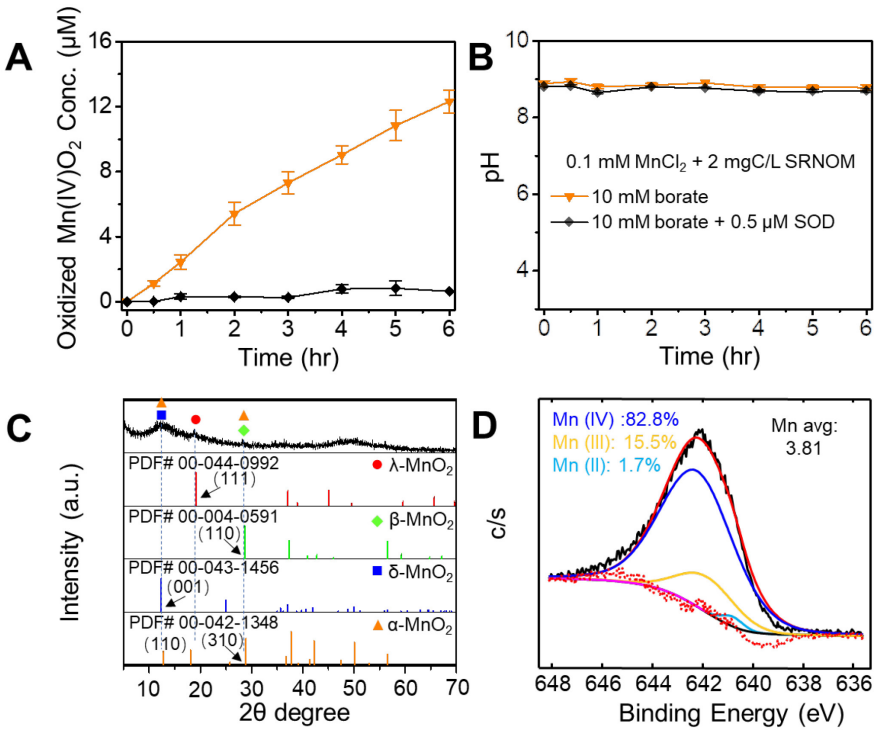

188

189 **Fig. 2.** Photochemical Mn oxidation by SRNOM at steady pH. (A) Oxidized Mn concentration
190 and (B) pH values during photolysis of solution containing 0.1 mM $MnCl_2$, 2 mgC/L SRNOM,
191 and 10 mM borate buffer at pH 9.0; and 0.1 mM $MnCl_2$, 2 mgC/L SRNOM, 10 mM borate buffer,
192 and 0.5 μM SOD at pH 9.0. Error bars represent the standard deviation from at least duplicate tests.
193 (C) HRXRD spectra of the formed Mn oxide solids under the condition of the above solution. (D)
194 Average Mn oxidation state of Mn $2p_{3/2}$ spectra calculated via Gaussian−Lorentzian fitting of
195 formed Mn oxide solids. At least duplicate tests were conducted for the characterization.

196

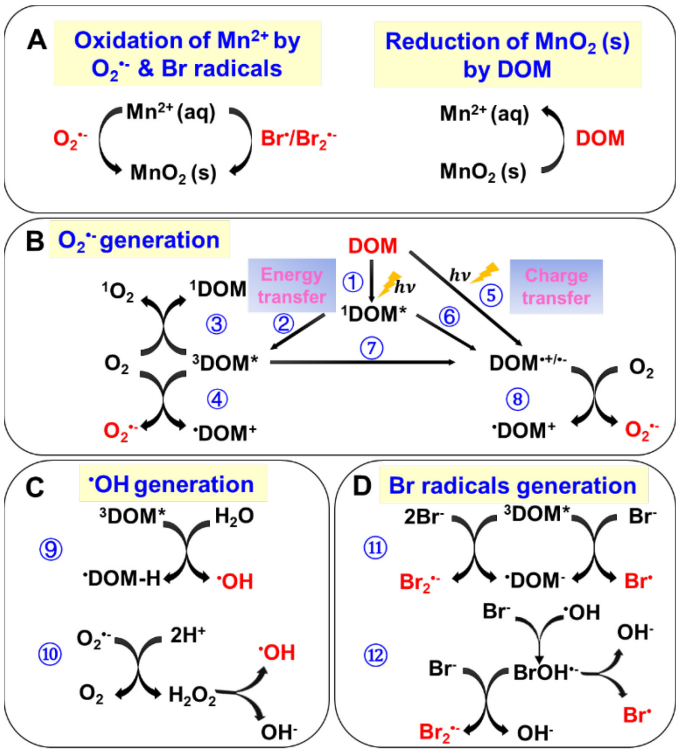

197

198 **Scheme 1.** Schematics of the pathways of Mn^{2+} oxidation, MnO_2 reduction, and the generation
199 pathways of reactive oxygen species and reactive bromide radicals during photolysis of DOM and
200 bromide ions. (A) Mn^{2+} oxidation by reactive oxygen species and reactive bromide radicals, and
201 MnO_2 reduction by DOM. (B) Chain reactions in the generation of $O_2^{\bullet-}$. (C) Chain reactions in the
202 generation of $^{\bullet}OH$. (D) Chain reactions in the generation of bromide radicals. Steps 1–8 and 10 are
203 based on references (Dalrymple et al. 2010, McNeill and Canonica 2016, Zafiriou 1977, Zafiriou
204 et al. 1984). Steps 9, 11, and 12 are based on references (De Laurentiis et al. 2012, Jammoul et al.
205 2009, Parker and Mitch 2016).

206

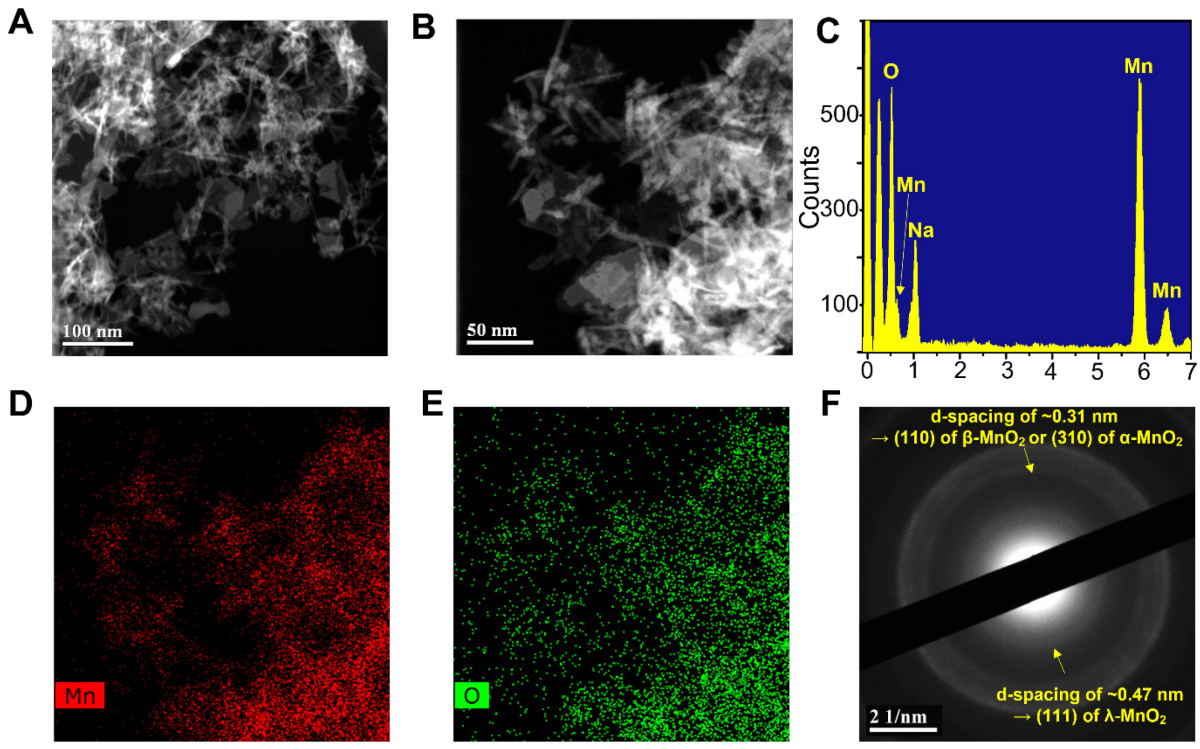

Fig. 3. Morphologies of the formed Mn oxides. (A,B) Representative HAADF-STEM images of Mn oxide solids formed by photolysis of solution containing 0.1 mM $MnCl_2$, 2 mgC/L SRNOM, and 10 mM borate buffer at pH 9.0. (C-E) STEM-EDX spectra and elemental mapping of Mn and O collected from (B). (F) SAED patterns were taken in the TEM mode in the area of (B), which confirmed the formation of λ-MnO_2, and β-MnO_2 or α-MnO_2. At least five different spots in the TEM grids were measured.

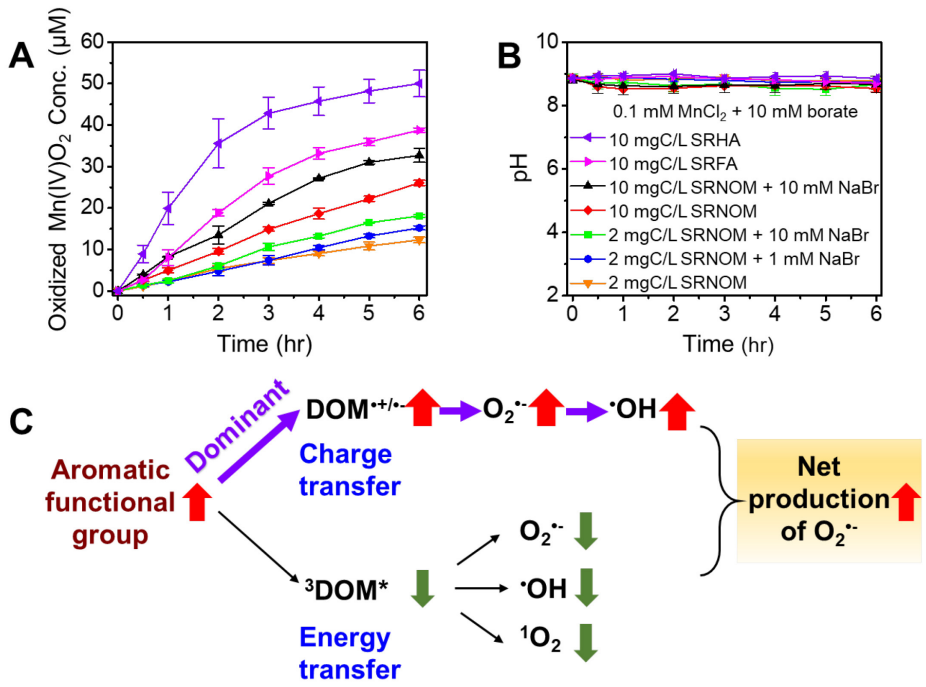

214

215 **Fig. 4.** Effects of concentrations of SRNOM, halide ions, and composition of DOM on Mn
216 oxidation. All experiment conditions contained 0.1 mM $MnCl_2$ and 10 mM borate buffer (pH 9.0).
217 (A) Oxidized Mn concentrations and (B) solution pH with experimental time under the conditions
218 of 0.1 mM $MnCl_2$, 10 mM borate buffer (pH 9.0): with 10 mgC/L SRHA; 10 mgC/L SRFA; 10
219 mgC/L SRNOM and 10 mM NaBr; 10 mgC/L SRNOM; 2 mgC/L SRNOM and 10 mM NaBr; 2
220 mgC/L SRNOM and 1 mM NaBr; and 2 mgC/L SRNOM. Error bars represent the standard
221 deviation from at least duplicate tests. (C) Schematic of the promotion of charge-transfer pathways
222 and inhibition of the energy-transfer pathway during photolysis of DOM with a higher amount of
223 aromatic functional groups. Upwards arrows indicate an increase in the generation, while
224 downwards arrows indicate a decrease. The thickness of the arrows indicates the extent of the
225 impact.